MRAS based speed sensorless control of PMSM Drive for urban electric vehicle

Bachir BENDJEDIA, Saad CHOUIREB

The University of Amar Thelidji of Laghouat, Algeria

The Faculty of Technology

Laboratory of Analysis and Control of Energy Systems and Power Networks (LACoSERE)

b.bendjedia@lagh-univ.dz, s.mhkf68@gmail.com

Abstract: This paper gives a clear visual appearance of the speed predictive control by a Model Reference Adaptive System (MRAS) observer for a Permanent-Magnet Synchronous Motor which is the heart of the electric vehicle's powertrain, The proposed approach used is Field Oriented Control (FOC) of the PMSM drive in case of speed sensor failure and the importance of substituted it by MRAS observer system to ensure the continuity of precaution situation drive and even get rid of its problems at all, thus improve the reliability of electric vehicle powertrain system and securing drivers and pedestrians from dangers.

The performances and robustness tests of the traction chain are achieved by real scenarios (driving cycles) such as NEDC, SFTP US06, and JP-15 combined with the vehicle dynamic model. This effectiveness study of (PMSM) drives enhanced by an observer in an electric car application confirms the high estimation accuracy and robustness of torque control of the proposed sensorless approach in several real road situations.

Keywords: Sensorless control, MRAS, Driving Cycle, NEDC, US06, JP-15, electric vehicle, observer, Permanent Magnet Synchronous Motor (PMSM).

1. Introduction

Recently, the interest in performance improvement of electric vehicles has increased greatly due to the hydrocarbon-fueled vehicles problems. For that, several research laboratories and industries develop various ideas to improve the performance of electric vehicles (Degaa et al., 2020), More developments are required to make EVs competitive. The main challenges are related directly to the cost, durability, and security (Bendjedia et al., 2020). These barriers are depended on the control and energy management strategies of the powertrain.

Generally, a high-accuracy mechanical position/speed sensor is necessary for excellent control, which also adds to the cost and complexity and reduces the reliability of the drive system. Therefore, the control system without mechanical position sensors, known as position/speed sensorless control of AC motors, is an appropriate replacement for this system. There are different types of electric motors that can be utilized for electric vehicles (Permanent Magnet Synchronous Motor, Induction Motor, Permanent Magnet Brushless DC Motor, Switched Reluctance Motor ...etc.). Installing mechanical sensors for example in permanent magnet synchronous motors increase cost, structure, and weight. To solve these problems, there are several techniques cover the real-time tracking and estimation of rotor speed, such as MRAS technology (Chen et al., 2021), which has many researches works that dealt with the control and observation strategies (Bendjedia et al., 2023). For implement it in the electric vehicle should prove it first in a virtual environment under real situations. There are two steps for the MRAS estimation strategy (Yuan et al., 2012): estimation based on measured voltage to create an estimated current through the PMSM model and estimation based on measured current to determine the estimated speed, which will be used to improve effectively the control accuracy of PMSM for electric vehicles.

To achieve better dynamic performance, the FOC strategy will allow for the separation of the flux and torque produced by currents enabling them to be controlled independently. These typically use proportional-integral (PI) controllers besides using pulse width modulation (PWM), this allows electric motors to operate smoothly in different conditions (the full speed range, full torque at zero speed). Also, it can deliver fast acceleration and deceleration of the motor (STMicroelectronics, 2022).

https://doi.org/10.33436/v33i3y202303

The objective of this paper is to support the powertrain when a fault suddenly happens and isolate the sensors faults at their incipient stage and perform its function by estimation for the prevention. For this purpose, the work goes from theoretical studies toward simulation validation through the modelling of the whole system.

In this paper, to check the performance robustness of the sensorless PMSM control based on MRAS observer different standard driving cycles were used. The first part presents the technical specification of a real vehicle in terms of driving cycles and dynamic model, then, MRAS observer design (Singh et al., 2017; Wu et al., 2017), and finally the results of the simulation which show the estimation performances in a variety of drive operations for a PMSM drive followed by a conclusion.

2. Technical specifications

2.1. Vehicle dynamic model

The electric vehicle model considers the applied forces during the rolling on the road. There are four force components represented in Figure 1: Aerodynamic Drag Force, Rolling Resistance, Force due to road profile, and Force due to acceleration.

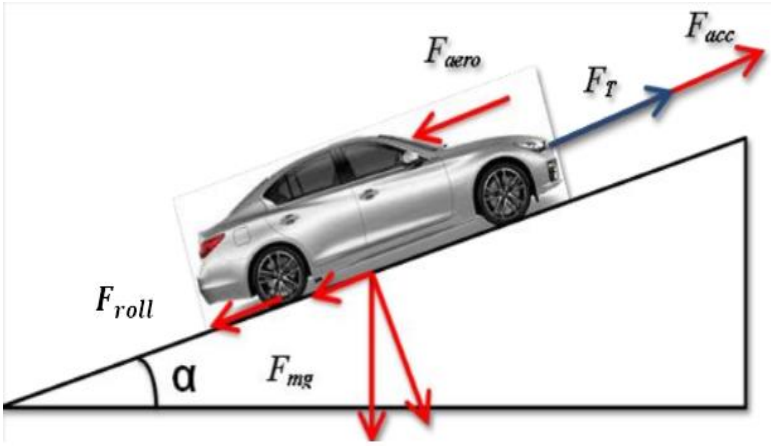

Figure 1. Forces applied to an electric vehicle (Bendjedia et al., 2022)

The total force form is written as:

$$F_T = F_{slope} + F_{aero} + F_{roll} + F_{acc} \tag{1}$$

Aerodynamic Drag Force:

$$F_{aero} = \frac{\rho A_F C_d}{2} V_{ev}^{\ 2} \tag{2}$$

Where ρ is the mass density of air, C_d is the aerodynamic drag coefficient, and A_F is the equivalent frontal area of the vehicle. The mass density of air is equal to ρ = 1.225 kg/m^3 at the commonly used standard set of conditions (15°C and a 101.32 kPa), g the acceleration of gravity and m_v the vehicle mass, C_0 Rolling resistance coefficient in a dynamic state and C_1 in a static state.

Force due to road profile:

$$F_{slope} = m_v g \sin\alpha \tag{3}$$

Force due to acceleration:

$$F_{acc} = m_v \frac{dV_{ev}}{dt} \tag{4}$$

Rolling Resistance:

$$F_{roll} = m_v g (C_0 + C_1) V_{ev}^{\ 2} \tag{5}$$

The power at the wheel P_{EV} can be expressed by:

$$P_{EV} = T_T \Omega_{roll} \tag{6}$$

The total traction torque T_T and the rotation speed of the wheel Ω_{roll} :

$$T_T = F_T r \tag{7}$$

$$\Omega_{roll} = \frac{V_{ev}}{r} \tag{8}$$

With: r the radius of the wheel.

Finally, we have:

$$P_{EV} = F_T V_{ev} \tag{9}$$

The vehicle considered in our work is the urban type, it's the Bluecar vehicle, represented in Figure 2, and the parameters of this car are arranged in the Table 1.

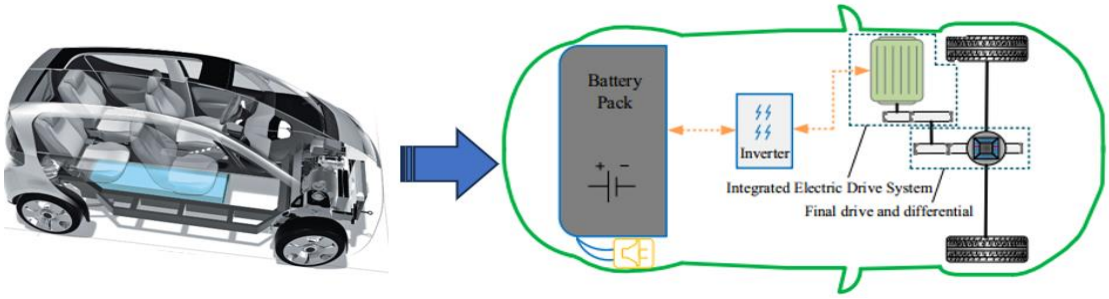

Figure 2. The Bluecar vehicle with the Structure diagram of an electric vehicle power transmission system equipped with an integrated electric drive system (Green Car Congress, 2015; Hu et al., 2020)

Table 1. Parameters of Bluecar type urban electric vehicle (Bendjedia et al., 2022)

VE Parameters	**value**
Vehicle mass (m_v)	820 kg
gravity force (g)	9.81 m/s^2
radius of a wheel (r)	0.33 m
Air density (ρ)	1.2 kg/m^3
Front area (AF)	2.75 m^2
Air penetration coefficient (C_x)	0.3
Rolling resistance coefficient in the dynamic state (C_0)	1.6e-6
Rolling resistance coefficient in a static state (C_1)	0.008
Incline angle of the road (α)	2.5%

2.2. Transmission and mechanical reducer

The electric vehicle power begins with a motor. It is transferred from the motor to the reducer adjusts the number of revolutions by the motor as shown in Figure 3 and is converted to the appropriate speed and torque for transmission to the tires. This procedure is more safely for electric motors and more efficient in electric vehicles.

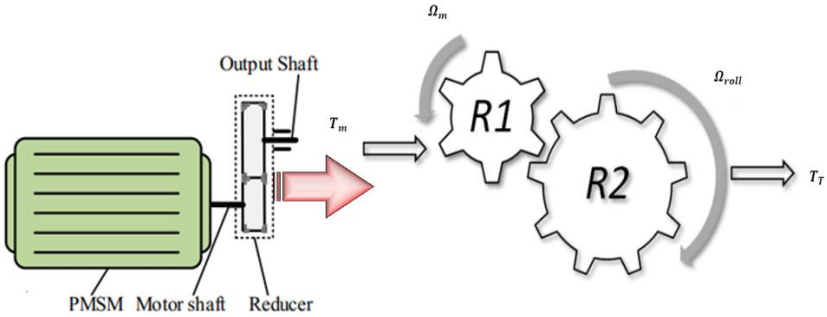

Figure 3. The gear mechanism (Bendjedia et al., 2022; Hu et al., 2020)

$$T_T = g_{dr} T_m \tag{10}$$

$$\omega_m = \frac{1}{g_{dr}} \omega_{roll} \tag{11}$$

g_{dr} : The gear ratio

T_T : is the wheel Torque

T_m : is the Motor Torque

ω_m : is the Motor speed $\omega_m = P\Omega_m$

ω_{roll} : is the wheel speed $\omega_{roll} = P\Omega_{roll}$

P : the number of machine pole-pairs

2.3. Driving Cycles

The European Driving Cycles, US Driving Cycles, and Japanese Driving Cycles are commonly used to evaluate a vehicle's performance in different countries. hence few different testing needs, they are generally differentiated by urban and highway driving cycles for light-duty vehicles.

2.3.1. North European Driving Cycles (NEDC)

Being the shortest distance and quickest drive cycle, the NEDC drive cycle includes four repetitions of the UDC driving cycle that we will use in our experiment and a segment of the EUDC driving cycle, as shown in Figure 4, the repetitions are devised to represent urban driving conditions, which maximum speed up to 120Km/h.

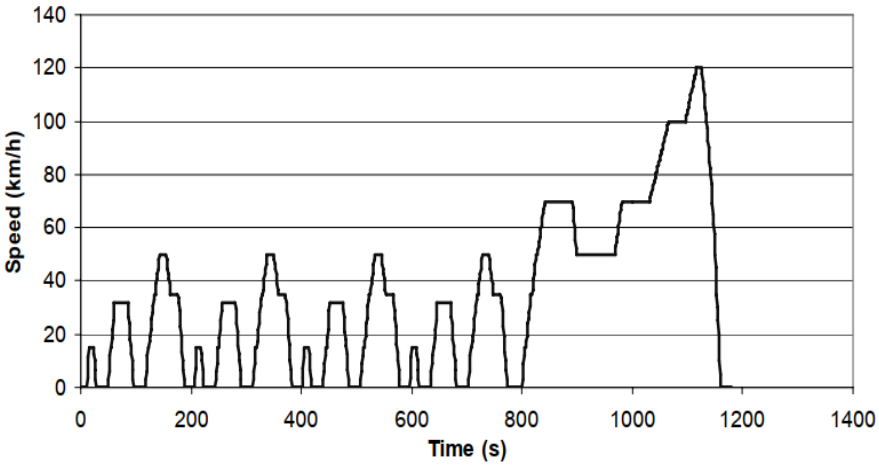

Figure 4. Velocity-time graph for the NEDC Driving Cycle (Barlow et al., 2009)

2.3.2. US06 Supplemental FTP

Supplemental Federal Test Procedure (SFTP or US06) driving cycle The US06 was used to reflect aggressive high-speed and high-acceleration driving behavior. The US06 driving cycle shown in Figure 5, is a high-speed/quick acceleration loop that lasts 10 minutes, covers 8 miles (13 km), averages 48 mph (77 km/h), and gets a maximum speed of 80 mph (130 km/h). Including four stops, and acceleration maximizes at a rate of 8.46 mph per second (13.62 km/h.s).

The higher acceleration rates and speeds of the US06 cycle led to higher motor loads.

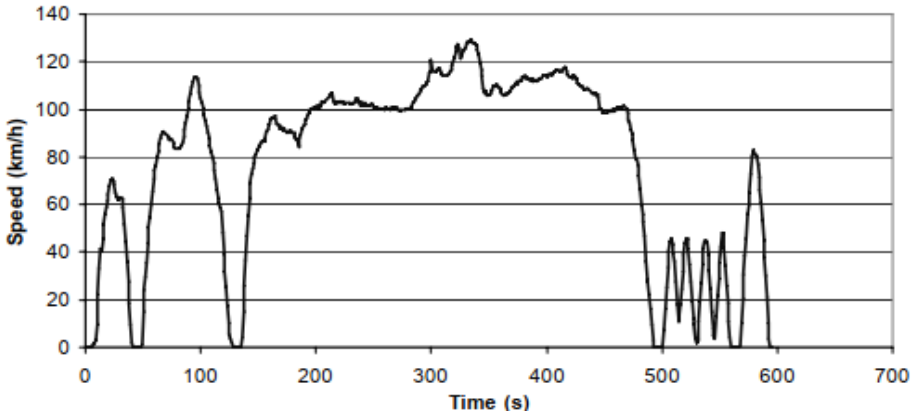

Figure 5. Velocity-time graph for the US FTP Driving Cycle (Barlow et al., 2009)

2.3.3. JP 10-15 Mode

The 10–15 mode driving cycle test for light duty vehicles in Japan, the test is achieved on a dynamometer and consists of 25 tests that cover acceleration, steady running, and deceleration, as shown in Figure 6 and simulates typical Japanese urban and/or expressway driving conditions. The cycle represents a 2.6-mile (4.16 km) route with an average speed of 14.1 miles/h (22.7 km/h), a maximum speed of 43.5 miles/h (70 km/h), and a duration of 660 seconds.

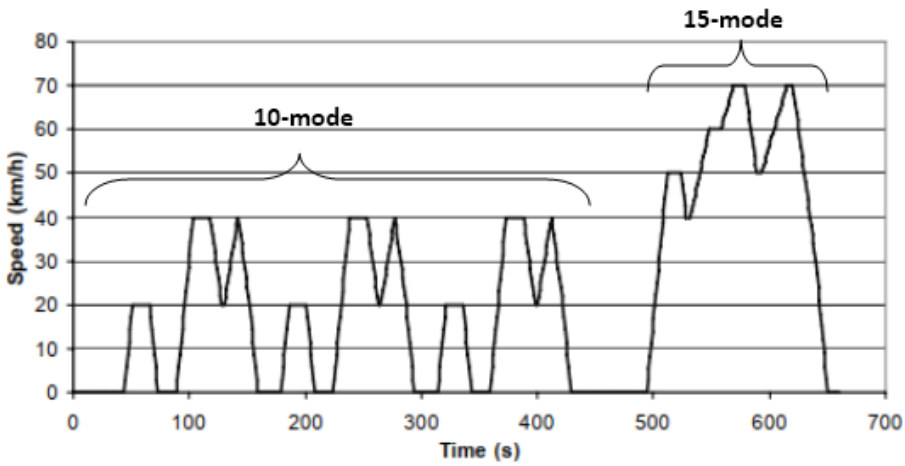

Figure 6. A velocity-time graph for the JP 10-15 Driving Cycle (Barlow et al., 2009)

3. FOC control strategy and MRAS observer design

Figure 7 shows a block diagram that outlines the MRAS-based sensorless vector control setup for the PMSM drive, which can operate at different speeds. The control blocks work together to ensure that the PMSM generates the necessary torque and achieves optimal dynamic performance.

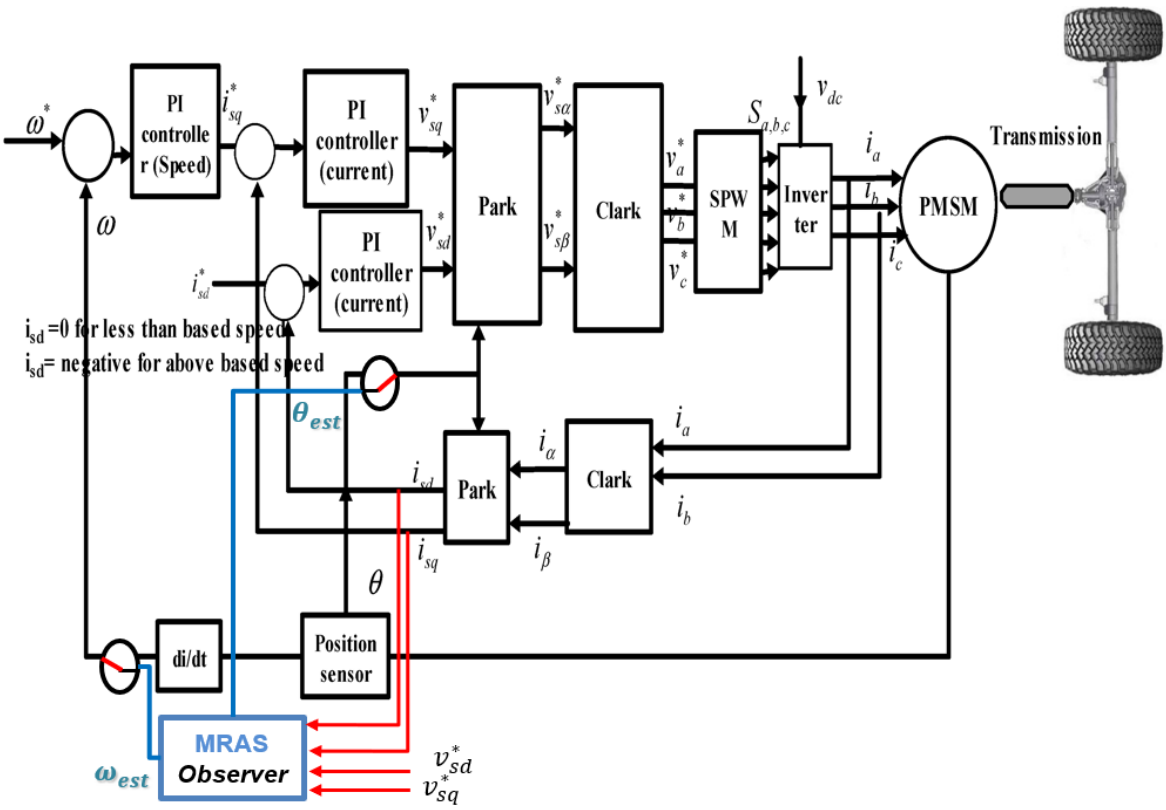

Figure 7. Field Oriented Control of Permanent Magnet Synchronous Motor without using a rotor position sensor (Murali et al., 2021)

1. The actual rotor speed information acquires by the speed sensor after a failure happens MRAS observer takes the sensor's place and provides the necessary information.
2. The reference speed and actual sensed/estimated speed are compared and the error signal is fed to the speed PI controller for generating a q-axis current.
3. Comparing the currents i_{sq} and i_{sd} with their reference values and the error signals serve as inputs to their respective PI controllers in the inner loop. This generates *d* and *q* axis voltage reference voltages.
4. V_{sd} and V_{sq} are converted into three-phase reference voltages by inverse transformations (Clarke's and Park's matrices are used for these transformations).
5. A two-level inverter compares them with a high-frequency carrier signal (sinusoidal PWM) to generate appropriate firing pulses for the six bidirectional switches of the inverter.
6. Mechanical speed (Ω_m) is calculated by the observer after every discrete PWM cycle.

3.1. Model reference adaptive vector system (MRAS)

3.1.1. Determination of the Reference Model and the Adjustable Model

The stator current model of PMSM in the d-q axis system is only related to its speed, so choose the current model as the adjustable model:

The Reference Model:

$$\frac{di_d}{dt} = \frac{R_s}{L_s} i_d + \omega_m i_q + \frac{1}{L_s} v_{sd}^* \tag{12}$$

$$\frac{di_q}{dt} = \frac{R_s}{L_s} i_q - \omega_m i_q - \frac{\lambda_m}{L_s} \omega_m + \frac{1}{L_s} v_{sq}^* \tag{13}$$

$$\frac{d}{dt}\begin{bmatrix} i_d + \dfrac{\lambda_m}{L_q} \\ i_q \end{bmatrix} = \begin{bmatrix} -\dfrac{R_s}{L_s} & \omega_m \\ -\omega_m & -\dfrac{R_s}{L_s} \end{bmatrix} \begin{bmatrix} i_d + \dfrac{\lambda_m}{L_s} \\ i_q \end{bmatrix} + \frac{1}{L_s}\begin{bmatrix} v_{sd}^* + \dfrac{R_s \lambda_m}{L_s} \\ v_{sq}^* \end{bmatrix} \tag{14}$$

Let:

$$i_d' = i_d + \frac{\lambda_m}{L_q} \qquad i_q' = i_q \qquad v_{sd}^{*\prime} = v_{sd}^* + \frac{R_s \lambda_m}{L_s} \qquad v_{sq}^{*\prime} = v_{sq}^*$$

To make the system stable with two variables and assume in the adjustable model that the speed is an input.

The Adjustable Model:

$$\frac{d}{dt}\begin{bmatrix} i_d' \\ i_q' \end{bmatrix} = \begin{bmatrix} -\dfrac{R_s}{L_s} & \omega_m \\ -\omega_m & -\dfrac{R_s}{L_s} \end{bmatrix} \begin{bmatrix} i_d' \\ i_q' \end{bmatrix} + \frac{1}{L_s}\begin{bmatrix} v_{sd}^{*\prime} \\ v_{sq}^{*\prime} \end{bmatrix} \tag{15}$$

3.1.2. The adaptive law

The adaptive law generally selects the form of proportional plus integral. According to the Popov hyperstability theory. The model reference adaptive system is designed. It can not only make the adjustable model approach the reference model but also can guarantee the system's stability, a block diagram of MRAS observer shown in Figure 8.

$$\omega_m = \int_0^t k_i \left(i_d i_q - i_q i_d - \frac{\lambda_m}{L_s}(i_q - i_q) \right) d\tau + K_p \left(i_d i_q - i_q i_d - \frac{\lambda_m}{L_s}(i_q - i_q) \right) \tag{16}$$

The above equation (16), i_d and i_q can be calculated from an adjustable model equation, i_d and i_q will be obtained by measurement (Zhao & Leidhold, 2022) and the proportional and integrator gains of the adaptation mechanism (K_p = 0.1; K_i = 10000).

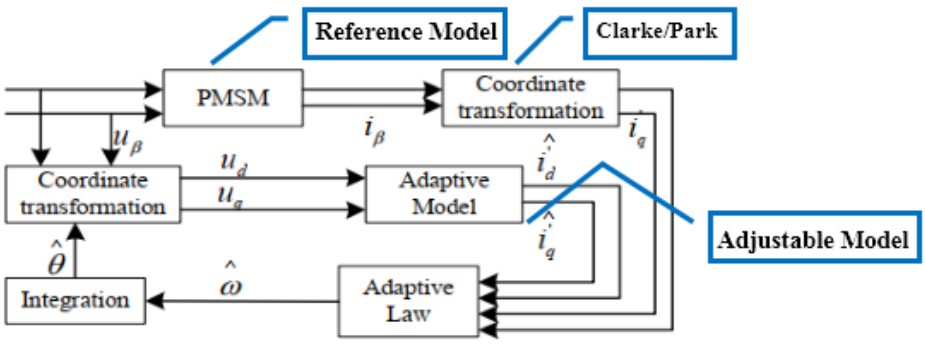

Figure 8. Block diagram of MRAS observer for PMSM sensorless vector control (Wu et al., 2017)

4. Simulation results

In order to check the MRAS performance on the electric vehicle model, three different cycles were used: The US06 Supplemental Federal Test Procedure (SFTP), The Modified New European Driving Cycle, and the Japanese 10-15 mode driving cycle which represent diverse levels of highway and city traffic. A PMSM 60kW was chosen whose parameters are indicated in Table 1 presented on (Hu et al., 2020).

A white noise signal was added to the speed sensor feedback at a certain time when this perturbation persists during 5s with a variance of 45 and a mean value of 5. After that, the speed sensor was replaced with a MRAS observer for each test to prevent the PMSM drive failure.

4.1. US06 Supplemental FTP

The following figures show the response results of our traction chain with the vector control technique (with sensor / without sensor) There is a 5-second interval [50s.55s] between the failure happen and the moment when the observer starts work shown in Figure 9:

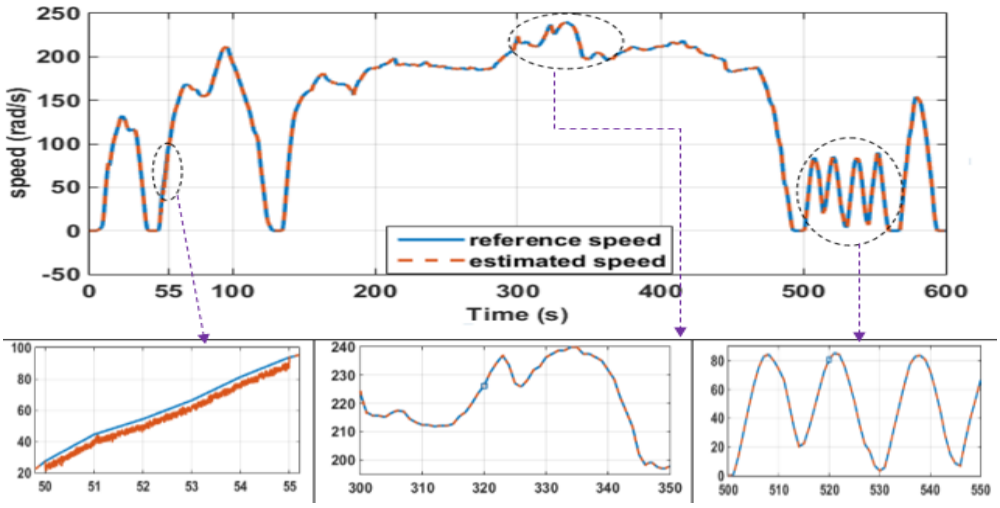

Figure 9. Vehicle Speed simulation results in rad/s, with speed sensor failure at the 50s

A basic operation of the motor may be seen when the vehicle accelerated quickly, the motor speed increased to around 240 rad/s (2292 tr/min) and generated high electric power of around 58KW shown in Figure 11. At t=50s we supposed the speed sensor break down and it took a few seconds until t=55s, the observer takes the speed sensor function and complete the control loop by estimating the speed and terminating the drive cycle.

In the start/stop section, the speed reaches a low value and the observer shows a good response, since the torque is softened as shown in Figure 10, the control system recovers rapidly, bringing the speed back to the desired range.

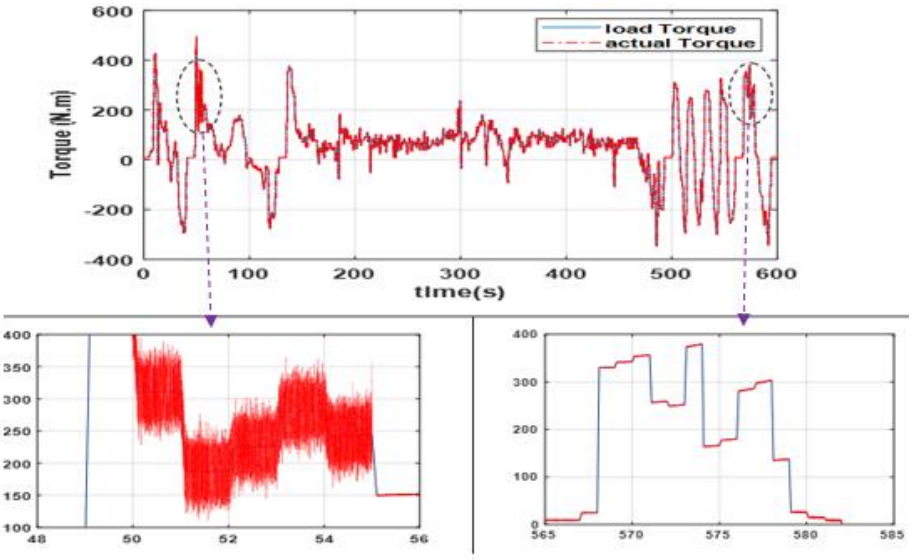

Figure 10. Vehicle Torque simulation results in N.m, with speed sensor failure at the 50s

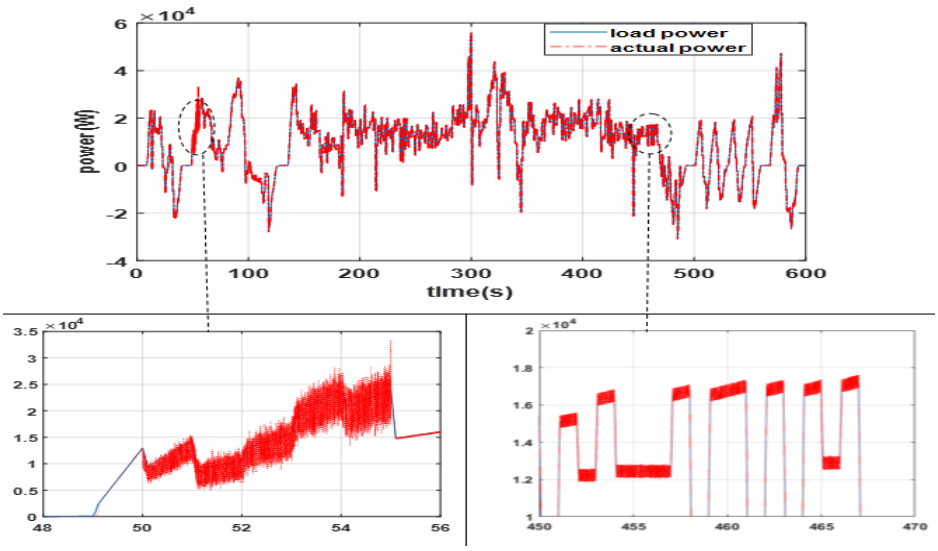

Figure 11. Vehicle Power simulation results in W, with speed sensor failure at the 50s

4.2. JP 10-15 Mode

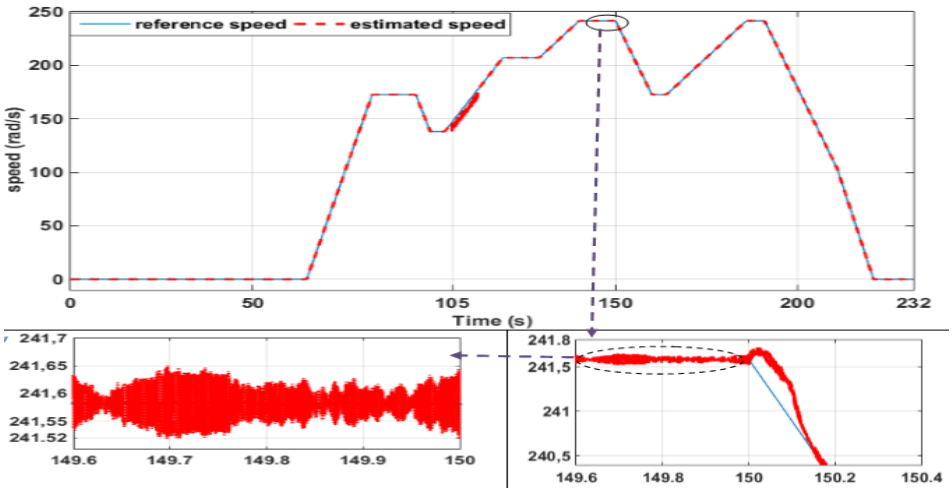

Figure 12. Vehicle Speed simulation results in rad/s with speed sensor failure at the 105s

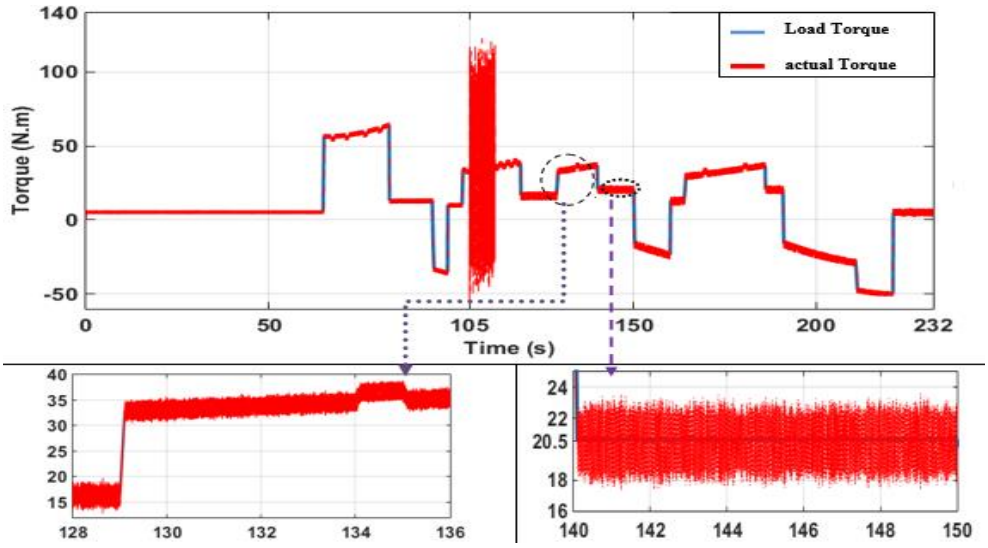

Figure 13. Vehicle Torque simulation results in N.m, with speed sensor failure at the 105s

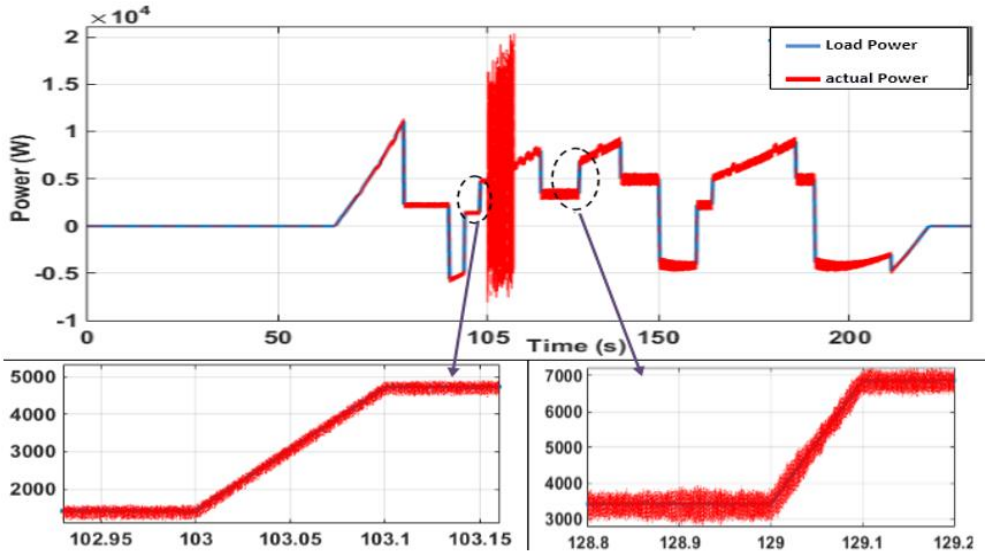

Figure 14. Vehicle Power simulation results in W, with speed sensor failure at the 105s

The MRAS observer during the first 75 s of a JP 05 drive-cycle and in compared conditions with and without speed sensor Figure 12 achieving a good velocity tracking performance.

Figure 13 compares the vehicle motor torque constrained between ± 65Nm, Figure 14 compares the power which achieved in the two conditions. the maximum power reaches 11KW.

4.3. M-NEDC

The Modified New European Driving Cycle (M-NEDC) implements the standardized European driving cycle for the extra-urban part as shown in Figure 15.

The comparison between the required torque and the actual is shown in Figure 16 and required vehicle power and the available power from the energy source with the M-NEDC drive cycle pattern are shown in Figure 17. The maximum amount of power consumed by the vehicle is 60 KW.

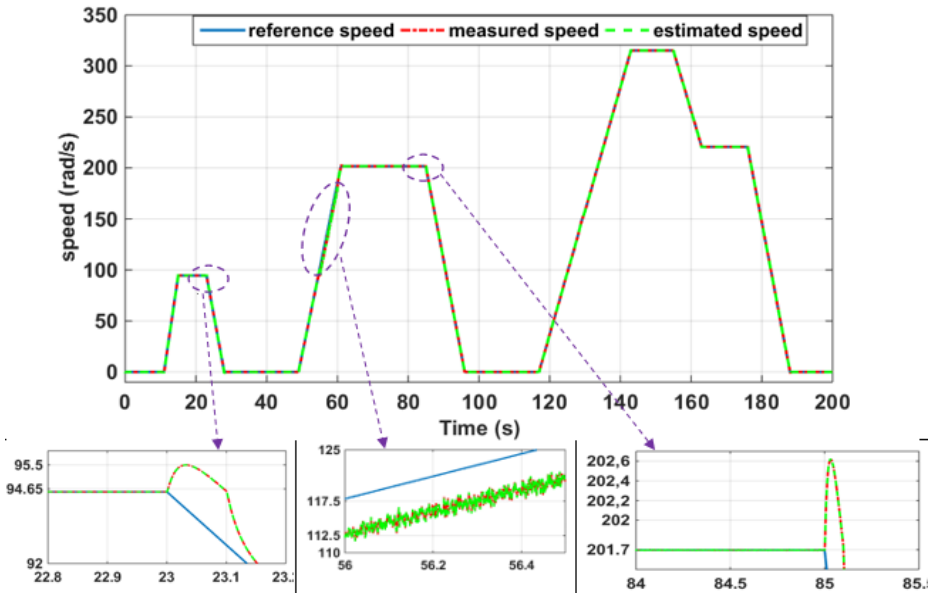

Figure 15. Vehicle Speed simulation results in rad/s, with speed sensor failure at the 55s

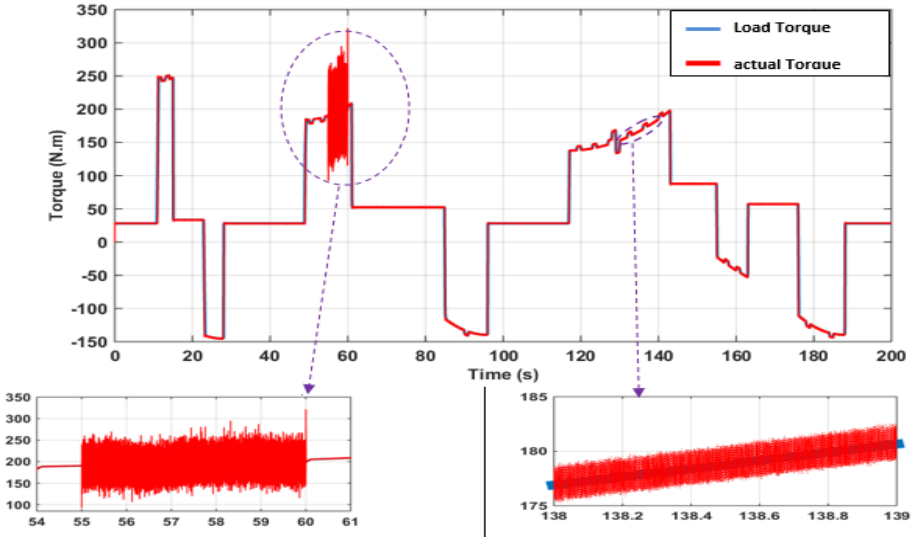

Figure 16. Vehicle Torque simulation results in N.m, with speed sensor failure at the 55s

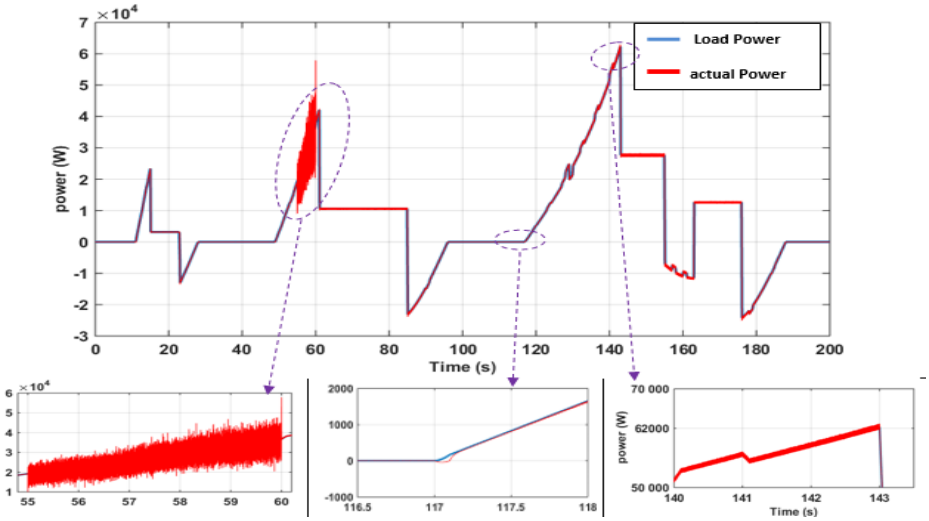

Figure 17. Vehicle Power simulation results in W, with speed sensor failure at the 55s

4.4. General discussion

The performances of the sensorless control by MRAS observer strategies are investigated using the M-NEDC drive cycle, JP-15 drive cycle, and US06 drive cycle. The M-NEDC drive cycle features low-speed urban driving with frequent stops, the JP-15 drive cycle is characterized by frequent stop-and-go traffic and very low speed, which represents a congested urban driving situation. and a supplemental test US06 drive cycle is developed to test vehicles at high speeds and high accelerations during aggressive driving conditions. The speed profiles of these three test drive cycles helped us greatly in evaluating the observer application and determining the limits of its work.

Speed figures show that the velocity tracking is satisfactory, the difference between the reference and estimated speed is small enough to be acceptable. One is composed of various driving modes of constant acceleration, and deceleration (like the M-NEDC), The other type is obtained from actual driving data and is referred to as the “real world” cycle. Such cycles are the SFTP-US06 and the JP-05. The real-world cycles are more dynamic, in this study, it is supposed that the power demand of the drive cycle will be provided by the electric drive train. It can be seen from the power figures that the maximum power available from the motor is approximately 60 kW. Summarizing the work and advantages for the MRAS observer and control performance in the following points:

- Perfect speed tracking with small errors and high accuracy;
- Large torque capability at low speeds;
- High torque and power control response;
- Tracking capability with quick acceleration/deceleration;
- Four-quadrant operation. When the wheel power command is negative, the motor is shut off without delivering power, and the battery is charged by regenerative braking;
- Good response with frequent start/stop operation;
- High overload capacity from zero to maximum speed;
- Production of constant torque at zero speed;
- Small torque oscillations.

5. Conclusion

This paper has been dedicated to the application of the FOC control techniques with the scenario of the speed sensor failure on the Traction chain of a real urban-type vehicle in the beginning, an overview of technical specifications out of driving cycles, the dynamic model and the reducer to help update the torque and vehicle speed was touched. then. by using these last two parameters, the load torque setpoints of the mechanical speed to the motor were applied, then MRAS observer design was discussed and subsequently, the control observation technique was applied.

The simulation results obtained have proven the vector control ensures acceptable performance in terms of stability and tracking of the setpoint and its robustness is good, especially concerning the rejection of disturbances. It is noted that in terms of precision speed and robustness are ensured by the MRAS observer compared to the speed sensor mode. These performances are reflected in the comfort of the car as well as the performance of the traction chain.

REFERENCES

Barlow, T.J., Latham, S., McCrae, I.S. & Boulter, P.G. (2009) A reference book of driving cycles for use in the measurement of road vehicle emissions. Version 3. TRL Limited, Published Project Report PPR 354.

Bendjedia, B. & Chouireb, S. (2023) Comparative Study Between Sensorless Vector Control of PMSM Drives based on MRAS, SMO and EKF Observers. In *2023 1st International Conference on Advances in Electronics, Control and Communication Systems (ICAECCS), Bilda 1 University, March 6-7, 2023, Bilda, Algeria*. IEEE. pp. 1-6.

Bendjedia, B., Baadj, L. & Ibrahimibrahimi, A. (2022) Sliding Mode Control of PMSM Drive for Lightweight Electric Vehicles. In *2022 19th International Multi-Conference on Systems, Signals & Devices, SSD, May 6-10, 2022, Setif, Algeria*. IEEE. pp. 2109-2114.

Bendjedia, B., Rizoug, N. & Boukhnifer, M. (2020) Real Time Implementation of Frequency Separation Management Strategy of Hybrid Source for Fuel Cell Electric Vehicle Applications. In *2020 IEEE 14th International Conference on Compatibility, Power Electronics and Power Engineering (CPE-POWERENG) July 8-10, 2020, Setubal, Portugal*. IEEE. pp. 544-549.

Chen, Q., Tian, Y., Kang, S., Yu, Y., Ding, J. & Xie, Y. (2021) Sensorless Control of Permanent Magnet Synchronous Motor for Electric Vehicle Based on Phase Locked Loop. *International Journal of Automotive Technology*. 22(5), 1409-1414. doi: 10.1007/s12239-021-0122-3.

Degaa, L., Bendjedia, B., Rizoug, N., Saidane, A. & Belaidi, A. (2020) Comparative study between different energy storage technologies to design hybrid source supplying urban electric vehicles. In *2020 3rd International Conference on Computer Applications & Information Security, ICCAIS 2020, March 19-21, 2020, Riyadh, Saudi Arabia.* IEEE. pp. 1-6.

Green car Congres. (2015) Bolloré Bluecar EV being assembled at Groupe Renault plant in Dieppe. https://www.greencarcongress.com/2015/06/20150608 − bollore.html [Accessed: 13th January 2023].

Hu, J., Yang, Y., Jia, M., Guan, Y., Fu, C. & Liao, S. (2020) Research on harmonic torque reduction strategy for integrated electric drive system in pure electric vehicle. *Electronics.* 9(8), 1241. doi: 10.3390/electronics9081241.

Murali, A., Wahab, R.S., Gade, C.S.R., Annamalai, C. & Subramaniam, U. (2021) Assessing finite control set model predictive speed controlled PMSM performance for deployment in electric vehicles. *World Electric Vehicle Journal*. 12(1), 41. doi: 10.3390/wevj12010041.

Singh, S., Tiwari, A.N. & Singh, S.N. (2017) Sensorless speed estimation of PM synchronous motor drive using MRAS. In *2017 IEEE International WIE Conference on Electrical and Computer Engineering (WIECON-ECE), December 18-19, 2017, Dehradun, India.* IEEE. pp. 35-38.

STMicroelectronics. 3-phase Field Oriented Control (FOC). https://www.st.com/en/applications/industrial-motor-control/3-phase-field-oriented-control-foc.html [Accessed: 13th January 2023].

Wu, J., Wei, H., Zhang, Y. & Wei, H. (2017) Sensorless vector control of permanent magnet synchronous motor based on model reference adaptive system. In *2017 3rd IEEE International Conference on Computer and Communications (ICCC), December 13-16, 2017, Chengdu, China.* IEEE. pp. 2879-2883.

Yuan, Q., Yang, Z., Cui, L., Hu, T. & Lin, F. (2012) A Position Estimation Method Based on Modified Integrator of PMSM Sensorless Control for High-Speed Vehicles. In *Proceedings of the 1st International Workshop on High-Speed and Intercity Railways.* Springer, Berlin, Heidelberg. pp. 9-18.

Zhao, Z. & Leidhold, R. (2022) On the estimation error of position sensorless control of PM synchronous motors. *Energy Reports*. 8, 1059-1065. doi: 10.1016/j.egyr.2021.11.177.

Bachir BENDJEDIA – He recently received state engineer's degree in electrical engineering from the Amar Telidji University of Laghouat, Laghouat, Algeria, in 2010; After that, he received Magister's (Bac+7) degree in Electrical engineering from Polytechnic School of Algiers. In November 2015, he joined the ESTACA'LAB in Paris, France as a Research Assistant. He obtained his PhD from the University of Science and Technology–Houari Boumediene in November 2017. He is now a Professor with the Department of Electrical Engineering, in the University of Laghouat and an associate researcher with ESTACA'LAB laboratory in France. His research interests include Storage systems, power electronics converters, electric vehicles and renewable energy sources.

Saad CHOUIREB – He recently graduated with an electromechanical Master`s degree in 2022 at the University of Laghouat in Algeria. His main areas of interest are Advanced Control of AC Drives, including Vector, Sensorless, and Electric vehicles (EVs) control, Fault Diagnosis, Power Energy Conversion Systems and Renewable Energy Systems Control.